

**DEVELOPMENT OF ALKALI-ACTIVATED  
BINDER UTILIZING SILICO-MANGANESE  
FUME AND BLAST-FURNACE SLAG**

**MUHAMMAD NASIR**

**UNIVERSITI SAINS MALAYSIA**

**2021**

**DEVELOPMENT OF ALKALI-ACTIVATED  
BINDER UTILIZING SILICO-MANGANESE  
FUME AND BLAST-FURNACE SLAG**

by

**MUHAMMAD NASIR**

**Thesis submitted in fulfilment of the requirements  
for the degree of  
Doctor of Philosophy**

**May 2021**

## **ACKNOWLEDGEMENT**

### **IN THE NAME OF ALLAH, THE MOST GRACIOUS, AND THE MOST MERCIFUL**

All praises and thanks are due only to ALLAH Subhanahu Wa Ta'aala, for bestowing me patience, health and knowledge to accomplish the thesis successfully. May the peace and blessings of Allah Subhanahu Wa Ta'aala be upon Prophet Mohammed (Sal Allahu Alahi Wa Sallam), his household and companions.

I would like to thank Universiti Sains Malaysia (USM) for providing the needed support during the course of my PhD program. My sincere, profound and eternal gratitude is devoted to the Chairman of my thesis committee, Prof. Dr. Megat Azmi Megat Johari at USM for his kind supervision, constructive guidance and huge support throughout this research. I would like to extend my appreciation to my co-supervisor, Prof. Dr. Mohammed Maslehuddin at Centre of Engineering Research (CER), Research Institute (RI) at King Fahd University of Petroleum and Minerals (KFUPM) for his constant encouragement and support in provision of some materials, casting platform and valuable feedbacks. My immense gratitude goes to another co-supervisor, Assistant Prof. Dr. Moruf Olalekan Yusuf at Civil and Environmental Engineering Department of Hafr Al Batin University for his continuous guidance and constructive criticism. In addition, many thanks are due to Prof. Dr. Mamdouh Al-Harhi affiliated with Centre of Excellence in Nano Technology (CENT) and Chemical Engineering Department at KFUPM for giving access to the characterization tests in his laboratories.

Beside USM, my unalloyed appreciation goes to other multiple academic and R&D institutions, namely Civil and Construction Engineering Department at Imam

Abdulrahman Bin Faisal University (IAU), CER and CENT at RI in KFUPM, Department of Chemical Engineering at KFUPM and Halliburton at Dhahran Techno Valley (DTV) for facilitating the experimental work to fulfil the mission of obtaining my PhD degree. Special thanks are due to Gulf Ferro Alloys Co. (Sabayek) – A Metallurgical Plant located at Jubail Industrial Estate at Eastern Saudi Arabia and Saudi ReadyMix Concrete Co. located at Dammam Industrial City at Eastern Saudi Arabia for providing the silico-manganese fume and ground granulated blast furnace slag, respectively.

Messrs Sarath and Hatim of KFUPM as well as Dr. Waseem Razzak of Halliburton are highly appreciated for their assistance and comradeship in conducting some useful material characterization tests. My senior PhD or Post Doc. research fellows at USM including Dr. Mohammed Ibrahim, Dr. Syed Khaja Najamuddin and Dr. Mustafa Juma A. Mijarsh as well as a PhD researcher Dr. Adeyemi Adesina from University of Windsor are gratefully thanked for their moral support and sharing troubleshooting skills during different stages of my research. Dr. Walid Al-Kutti at IAU is also thanked for motivating and supporting me to pursue PhD degree.

My enormous appreciation goes to my parents, more especially the deposed soul of my amiable mother who passed to the world beyond in the course of this study. Unflinching support received from my siblings cannot be forgotten. All these acknowledgements cannot be completed without appreciating the psychological supports received from my wife and my children. Their unconditional love, encouragement, support and devotion during all stages of my life can never go into oblivion. Without their patience and prayers this modest contribution to Civil Engineering and Alkali-activated materials could not have been made.

**DEDICATED TO MY PARENTS & MY FAMILY**

## TABLE OF CONTENTS

<b>ACKNOWLEDGEMENT</b> .....	<b>ii</b>
<b>TABLE OF CONTENTS</b> .....	<b>iv</b>
<b>LIST OF TABLES</b> .....	<b>xiii</b>
<b>LIST OF FIGURES</b> .....	<b>xv</b>
<b>LIST OF SYMBOLS</b> .....	<b>xxiii</b>
<b>LIST OF ABBREVIATIONS</b> .....	<b>xxv</b>
<b>ABSTRAK</b> .....	<b>xxvii</b>
<b>ABSTRACT</b> .....	<b>xxix</b>
<b>CHAPTER 1 INTRODUCTION</b> .....	<b>1</b>
1.1 Background to the study.....	1
1.2 Problem statement .....	4
1.3 Significance of research .....	6
1.4 Objectives of research .....	8
1.5 Scope of the research.....	9
1.6 Organization of the thesis.....	10
<b>CHAPTER 2 LITERATURE REVIEW</b> .....	<b>12</b>
2.1 Preamble.....	12
2.2 Cement production and associated problems .....	13
2.3 Solid wastes generation and associated problems .....	16
2.3.1 Hazards of exposure to solid wastes .....	16
2.3.2 Landfilling and stockpiling problems .....	17
2.4 Manganese alloy production and associated problems .....	17
2.4.1 Ferroalloy production process.....	18
2.4.2 Mn concentration in the vicinity of some ferroalloy plants .....	22
2.4.3 Health problems associated with Mn exposure.....	23

2.5	Remedy of recycling solid wastes in construction industry .....	24
2.6	Alkali-activated binder (AAB) .....	25
2.6.1	Historical background .....	25
2.6.2	Chemistry of AAB .....	28
2.6.3	Mechanism of formation of AAB .....	30
2.6.4	Aluminosilicate source materials .....	33
2.6.5	Factors affecting the synthesis of alkaline activated binder.....	34
2.6.5(a)	Composition of precursor materials.....	34
2.6.5(b)	Composition and concentration of alkaline activators.....	38
2.6.5(c)	The importance of water in the synthesis of AAB .....	39
2.6.5(d)	Type and duration of curing .....	40
2.6.5(e)	Fineness of source materials .....	42
2.6.6	Durability of AAB under aggressive environments.....	44
2.6.6(a)	Durability of AAB under acidic environment .....	44
2.6.6(b)	Durability of AAB under sulphate environment .....	46
2.7	Challenges in the synthesis of AAB.....	50
2.8	Taguchi method for design of experiments.....	52
2.9	Research gap .....	54
<b>CHAPTER 3 MATERIAL AND METHODS.....</b>		<b>58</b>
3.1	Material .....	59
3.1.1	Precursor materials (PMs).....	59
3.1.2	Fine aggregate .....	60
3.1.3	Water .....	60
3.1.4	Alkaline activators.....	61
3.1.5	Chemical used in the durability studies.....	62
3.2	Methods.....	64
3.2.1	Characterization of PMs.....	65

3.2.1(a)	Colour and shape .....	65
3.2.1(b)	Strength activity index .....	66
3.2.1(c)	Particle size distribution .....	66
3.2.1(d)	Specific gravity .....	67
3.2.1(e)	Surface area and pore volume.....	67
3.2.1(f)	X-ray fluorescence spectroscopy .....	68
3.2.1(g)	Moisture content .....	69
3.2.1(h)	Loss on ignition .....	69
3.2.2	Taguchi method for designing and optimizing mix parameters.....	70
3.2.2(a)	Results validation and analysis using ANOVA/multilinear regression analysis/sum of square methods .....	73
3.2.3	Impact of GGBFS/PMs ratio.....	74
3.2.4	Effect of alkaline activators.....	75
3.2.5	Influence of curing methods.....	77
3.2.6	Resistance to sulfuric acid attack .....	79
3.2.7	Resistance to magnesium sulphate attack .....	80
3.2.8	Resistance to sodium sulphate attack.....	81
3.3	Specimen preparation .....	82
3.4	Curing.....	86
3.5	Exposure for durability studies .....	86
3.6	Evaluation of fresh, hardened and microstructural properties .....	88
3.6.1	Fresh properties .....	88
3.6.1(a)	Setting times .....	89
3.6.1(b)	Flow .....	90
3.6.2	Hardened properties .....	91
3.6.2(a)	Compressive strength.....	92
3.6.3	Durability characteristics.....	93

3.6.3(a)	Alkalinity .....	93
3.6.3(b)	Visual inspection .....	93
3.6.3(c)	Mass change.....	94
3.6.3(d)	Residual Compressive strength.....	94
3.6.4	Analytical tests .....	95
3.6.4(a)	Thermogravimetric analysis .....	95
3.6.4(b)	X-ray diffraction analysis .....	96
3.6.4(c)	Fourier transform infra-red spectroscopy .....	97
3.6.4(d)	Scanning electron microscopy and energy dispersive spectroscopy .....	98
<b>CHAPTER 4</b>	<b>RESULTS AND DISCUSSION.....</b>	<b>100</b>
4.1	Characterization of PMs .....	100
4.1.1	Physical properties .....	101
4.1.1(a)	Colour, shape, size, surface area and specific gravity .....	101
4.1.1(b)	Morphology .....	102
4.1.1(c)	Strength activity index.....	103
4.1.2	Chemical properties.....	104
4.1.2(a)	Composition.....	104
4.1.2(b)	Mineralogy.....	106
4.1.2(c)	Bond characteristics.....	107
4.1.3	Summary .....	108
4.2	Implementation of Taguchi method for designing and optimizing mix parameters .....	109
4.2.1	Compressive strength development .....	109
4.2.1(a)	Statistical analysis.....	111
4.2.2	Effect of factors on the compressive strength .....	113
4.2.2(a)	Effect of GGBFS to PMs ratio on the compressive strength (Factor A).....	113



4.2.2(b)	Effect of sand to PMs ratio on the compressive strength (Factor B).....	114
4.2.2(c)	Effect of NaOH molarity on the compressive strength (Factor C).....	114
4.2.2(d)	Effect of Na <sub>2</sub> SiO <sub>3</sub> /NaOH ratio on the compressive strength (Factor D).....	115
4.2.2(e)	Effect of AAs/PMs ratio on the compressive strength (Factor E).....	115
4.2.2(f)	Model development and factors contribution .....	116
4.2.3	Optimization and validation .....	118
4.2.4	Summary .....	119
4.3	Role of GGBFS/PMs ratio .....	119
4.3.1	Impact of GGBFS/PMs ratio on setting times .....	120
4.3.2	Impact of GGBFS/PMs ratio on flow .....	121
4.3.3	Impact of GGBFS/PMs ratio on compressive strength.....	122
4.3.4	Impact of GGBFS/PMs ratio on mineralogy.....	123
4.3.5	Impact of GGBFS/PMs ratio on bond characteristics.....	126
4.3.6	Impact of GGBFS/PMs ratio on thermogravimetry.....	127
4.3.7	Impact of GGBFS/PMs ratio on morphology and elemental composition .....	129
4.3.8	Summary .....	132
4.4	Effect of NaOH concentration and Na <sub>2</sub> SiO <sub>3</sub> /NaOH ratio .....	133
4.4.1	Impact of NaOH concentration and Na <sub>2</sub> SiO <sub>3</sub> /NaOH ratio on setting times and flow characteristics.....	133
4.4.2	Impact of uncombined activators on compressive strength .....	134
4.4.2(a)	Impact of uncombined activators on bond characteristics .....	135
4.4.2(b)	Impact of uncombined activators on morphology .....	136
4.4.3	Impact of combined activators prepared by varying NaOH concentration on compressive strength .....	138

4.4.3(a)	Impact of combined activators prepared by varying NaOH concentration on bond characteristics .....	138
4.4.3(b)	Impact of combined activators prepared by varying NaOH concentration on morphology and elemental composition.....	140
4.4.4	Impact of combined activators prepared by varying Na <sub>2</sub> SiO <sub>3</sub> to NaOH ratio on compressive strength .....	144
4.4.4(a)	Impact of combined activators prepared by varying Na <sub>2</sub> SiO <sub>3</sub> to NaOH ratio on bond characteristics .....	144
4.4.4(b)	Impact of combined activators prepared by varying Na <sub>2</sub> SiO <sub>3</sub> to NaOH ratio on morphology and elemental composition .....	146
4.4.5	Summary .....	148
4.5	Influence of curing methods and exposure to heat curing conditions.....	149
4.5.1	Impact of curing methods and varying binder type on the compressive strength.....	150
4.5.2	Impact of varying curing conditions on the compressive strength of blended mortar .....	151
4.5.2(a)	Impact of water-ponding on the compressive strength .....	152
4.5.2(b)	Impact of room temperature curing on the compressive strength .....	152
4.5.2(c)	Impact of oven-curing period at constant temperature on the compressive strength .....	153
4.5.2(d)	Impact of oven-curing temperature at constant period on the compressive strength .....	154
4.5.3	Impact of curing methods on the mineralogy.....	156
4.5.4	Impact of curing methods on the bond characteristics.....	158
4.5.5	Impact of curing methods on the morphology .....	161
4.5.6	Summary .....	165
4.6	Resistance to sulfuric acid attack .....	166
4.6.1	Residual compressive strength after exposure to pure H <sub>2</sub> O and 5% H <sub>2</sub> SO <sub>4aq</sub> .....	167

4.6.1(a)	Impact of GGBFS/PMs ratio on the 5% H <sub>2</sub> SO <sub>4aq</sub> resistance.....	168
4.6.1(b)	Impact of NaOH concentration on the 5% H <sub>2</sub> SO <sub>4aq</sub> resistance.....	168
4.6.2	Impact of GGBFS/PMs ratio and NaOH concentration on the morphology of specimens immersed in 5% H <sub>2</sub> SO <sub>4aq</sub> .....	169
4.6.3	Impact of GGBFS/PMs ratio and NaOH concentration on the physical structure of specimens immersed in 5% H <sub>2</sub> SO <sub>4aq</sub> .....	174
4.6.4	Impact of GGBFS/PMs ratio and NaOH concentration on the pH of 5% H <sub>2</sub> SO <sub>4</sub> solution.....	176
4.6.5	Impact of GGBFS/PMs ratio and NaOH concentration on the mass change of specimens immersed in 5% H <sub>2</sub> SO <sub>4aq</sub> .....	177
4.6.6	Impact of GGBFS/PMs ratio and NaOH concentration on the mineralogy of specimens immersed in 5% H <sub>2</sub> SO <sub>4aq</sub> .....	179
4.6.7	Impact of GGBFS/PMs ratio and NaOH concentration on the bond characteristics of specimens immersed in 5% H <sub>2</sub> SO <sub>4aq</sub> .....	182
4.6.8	Impact of GGBFS/PMs ratio and NaOH concentration on the elemental composition of specimens immersed in 5% H <sub>2</sub> SO <sub>4aq</sub> .....	184
4.6.9	Summary .....	186
4.7	Resistance to magnesium sulphate attack .....	186
4.7.1	Residual Compressive strength after exposure to pure H <sub>2</sub> O and 5% MgSO <sub>4aq</sub> .....	187
4.7.1(a)	Impact of GGBFS/PMs ratio on the 5% MgSO <sub>4aq</sub> resistance.....	188
4.7.1(b)	Impact of NaOH concentration on the 5% MgSO <sub>4aq</sub> resistance.....	189
4.7.2	Impact of GGBFS/PMs ratio and NaOH concentration on the morphology of specimens immersed in 5% MgSO <sub>4aq</sub> .....	189
4.7.3	Impact of GGBFS/PMs ratio and NaOH concentration on the physical structure of specimens immersed in 5% MgSO <sub>4aq</sub> .....	192
4.7.4	Impact of GGBFS/PMs ratio and NaOH concentration on the pH of 5% MgSO <sub>4</sub> solution .....	194
4.7.5	Impact of GGBFS/PMs ratio and NaOH concentration on the mass change of specimens immersed in 5% MgSO <sub>4aq</sub> .....	196

4.7.6	Impact of GGBFS/PMs ratio and NaOH concentration on the mineralogy of specimens immersed in 5% MgSO <sub>4aq</sub> .....	197
4.7.7	Impact of GGBFS/PMs ratio and NaOH concentration on the bond characteristics of specimens immersed in 5% MgSO <sub>4aq</sub> .....	201
4.7.8	Impact of GGBFS/PMs ratio and NaOH concentration on the elemental analysis of specimens immersed in 5% MgSO <sub>4aq</sub> .....	203
4.7.9	Summary .....	205
4.8	Resistance to sodium sulphate attack .....	205
4.8.1	Residual Compressive strength after exposure to pure H <sub>2</sub> O and 5% Na <sub>2</sub> SO <sub>4aq</sub> .....	206
4.8.1(a)	Impact of GGBFS/PMs ratio on the 5% Na <sub>2</sub> SO <sub>4aq</sub> resistance.....	207
4.8.1(b)	Impact of NaOH concentration on the 5% Na <sub>2</sub> SO <sub>4aq</sub> resistance.....	208
4.8.2	Impact of GGBFS/PMs ratio and NaOH concentration on the morphology of specimens immersed in 5% Na <sub>2</sub> SO <sub>4aq</sub> .....	208
4.8.3	Impact of GGBFS/PMs ratio and NaOH concentration on the physical structure of specimens immersed in 5% Na <sub>2</sub> SO <sub>4aq</sub> .....	211
4.8.4	Impact of GGBFS/PMs ratio and NaOH concentration on the pH of 5% Na <sub>2</sub> SO <sub>4</sub> solution.....	212
4.8.5	Impact of GGBFS/PMs ratio and NaOH concentration on the mass change of specimens immersed in 5% Na <sub>2</sub> SO <sub>4aq</sub> .....	214
4.8.6	Impact of GGBFS/PMs ratio and NaOH concentration on the mineralogy of specimens immersed in 5% Na <sub>2</sub> SO <sub>4aq</sub> .....	215
4.8.7	Impact of GGBFS/PMs ratio and NaOH concentration on the elemental composition of specimens immersed in 5% Na <sub>2</sub> SO <sub>4aq</sub> .....	218
4.8.8	Summary .....	220
<b>CHAPTER 5 CONCLUSIONS AND RECOMMENDATIONS.....</b>		<b>221</b>
5.1	Conclusions .....	221
5.1.1	Characterization of raw PMs.....	222
5.1.2	Taguchi method for designing and optimizing mix parameters...	223
5.1.3	Impact of GGBFS/PMs ratio.....	224

5.1.4	Effect of alkaline activators.....	225
5.1.5	Influence of curing methods.....	226
5.1.6	Resistance to sulfuric acid attack .....	228
5.1.7	Resistance to magnesium sulphate attack .....	229
5.1.8	Resistance to sodium sulphate attack .....	230
5.2	Recommendations .....	232
5.3	Suggestions for future research .....	233
	<b>REFERENCES.....</b>	<b>235</b>
	APPENDICES	
	LIST OF PUBLICATIONS	

## LIST OF TABLES

	<b>Page</b>
Table 2.1	Statistics of Mn concentration in the vicinity of some ferroalloy plants .....23
Table 2.2	Chemical compositions of various PMs.....36
Table 3.1	Particle size distribution of fine aggregate.....60
Table 3.2	Physico-chemical characteristics of sodium silicate .....61
Table 3.3	Factors and levels used in the Taguchi experimental design .....72
Table 3.4	Taguchi method of orthogonal arrays [L16 (4 <sup>5</sup> )] of the experimental design .....72
Table 3.5	Mix proportions prepared for trial mixtures .....72
Table 3.6	Mix proportions prepared for studying the impact of GGBFS/PMs ratio .....75
Table 3.7	Mix proportions prepared for studying the impact of alkaline activators .....76
Table 3.8	Molar composition of the mixtures for studying the impact of alkaline activators.....77
Table 3.9	Mix proportions for studying the impact of curing methods .....78
Table 3.10	Mix proportions for studying the resistance to sulfuric acid attack...80
Table 3.11	Mix proportions for studying the resistance to magnesium sulphate attack .....80
Table 3.12	Mix proportions for studying the resistance to sodium sulphate attack .....81
Table 3.13	Mixing procedure for traditional and alkali-activated binders.....83
Table 3.14	Specification of Vicat's apparatus and its accessories.....90
Table 4.1	Physical properties of the PMs..... 101

Table 4.2	Strength activity index of PMs.....	104
Table 4.3	Chemical composition of PMs using XRF .....	104
Table 4.4	Chemical composition of PMs using EDS.....	104
Table 4.5	Flow and compressive strength data of the trial AABs .....	110
Table 4.6	Analysis of variance results on 28-day compressive strength .....	112
Table 4.7	Model derived for predicting 28-day compressive strength of AABs.....	117
Table 4.8	Optimization of the factor's combination of AABs.....	118
Table 4.9	Interpretation of TG data of SiMnF-alone (M18) and optimum SiMnF-GGBFS blended (M17) AABs .....	128
Table 4.10	Elemental composition of SiMnF-alone (M18) and optimum SiMnF-GGBFS blended (M17) AABs .....	132
Table 4.11	Elemental composition of AABs prepared by varying NaOH concentration and Na <sub>2</sub> SiO <sub>3</sub> to NaOH ratio.....	143
Table 4.12	EDS data of AABs immersed in pure H <sub>2</sub> O and 5% H <sub>2</sub> SO <sub>4aq</sub> .....	185
Table 4.13	EDS data of AABs immersed in pure H <sub>2</sub> O and 5% MgSO <sub>4aq</sub> .....	203
Table 4.14	EDS data of AABs immersed in pure H <sub>2</sub> O and 5% Na <sub>2</sub> SO <sub>4aq</sub> .....	218

## LIST OF FIGURES

	<b>Page</b>
Figure 1.1	Number of publications on alkali-activated materials ..... 7
Figure 2.1	Comparison of cement and steel production with the population..... 14
Figure 2.2	Cement manufacturing process ..... 15
Figure 2.3	Greenhouse gasses (GHGs) emissions from cement production ..... 16
Figure 2.4	2009 statistics of world (a) Mn reserves and (b) production ..... 18
Figure 2.5	Flow chart detailing the production process of FeMn and SiMn at a typical ferroalloy plant ..... 20
Figure 2.6	Schematic illustration of flow of raw materials in a typical ferroalloy plant ..... 21
Figure 2.7	World Mn alloy production of different grades ..... 22
Figure 2.8	Classification of alkali-activated materials ..... 28
Figure 2.9	Conceptual model illustrating the formation of AAB..... 31
Figure 2.10	Conceptual model of alkaline activation of low calcium aluminosilicate precursor materials ..... 32
Figure 2.11	Morphology of (a) raw fly ash, (b) N-A-S-H gel, (c) Zeolite P, (d) Analcime ..... 37
Figure 2.12	Morphology of N-A-S-H and C-A-S-H gels..... 37
Figure 3.1	Flow chart showing the overall methodology of research ..... 59
Figure 3.2	Magnetic stirrer used for the preparation of NaOH <sub>aq</sub> ..... 62
Figure 3.3	Materials used for preparing the alkali-activated binders and exposure solutions: (a) SiMnF, (b) GGBFS, (c) FAG, (d) bag of NaOH flakes, (e) drum of Na <sub>2</sub> SiO <sub>3aq</sub> , (f) distillation unit for water, (g) bottle of H <sub>2</sub> SO <sub>4aq</sub> , (h) bag of MgSO <sub>4</sub> salt and (i) bag of Na <sub>2</sub> SO <sub>4</sub> salt ..... 64
Figure 3.4	Flow chart of tests conducted on precursor materials ..... 65



Figure 3.5	Particle size analyser used for measuring the particle size distribution of the PMs.....	67
Figure 3.6	Gas pycnometer used for measuring the specific gravity of the PMs .....	67
Figure 3.7	Surface area and pore size analyser used for measuring the surface area and pore volume of the PMs.....	68
Figure 3.8	X-ray fluorene spectrometer used for measuring the chemical composition of the PMs .....	69
Figure 3.9	Flow chart of the study on the alkaline activators.....	77
Figure 3.10	Flow chart of the study on the curing methods .....	79
Figure 3.11	Flow chart of the study on the resistance to chemical attacks .....	82
Figure 3.12	Picture gallery exhibiting the preparation of paste and mortar specimens .....	85
Figure 3.13	Pictorial view of specimens subjected to curing methods used: Ambient curing (left), water ponding (middle) and heat curing (right).....	86
Figure 3.14	Schematic of the exposure set-up: (a) plan view and (b) section AA .....	87
Figure 3.15	Pictorial view of specimens exposed to H <sub>2</sub> O and H <sub>2</sub> SO <sub>4aq</sub> .....	87
Figure 3.16	Pictorial view of specimens exposed to H <sub>2</sub> O and MgSO <sub>4aq</sub> .....	87
Figure 3.17	Pictorial view of specimens exposed to H <sub>2</sub> O and Na <sub>2</sub> SO <sub>4aq</sub> .....	88
Figure 3.18	Flow chart of tests conducted on AABs.....	88
Figure 3.19	Pictorial view of setting time test set-up on typical paste specimens .....	90
Figure 3.20	Pictorial view of flow table test set-up on typical mortar specimens .....	91
Figure 3.21	Pictorial view of compression machine (Left) and close-up view (Right) of testing on a typical mortar specimen.....	93

Figure 3.22	Picture gallery for preparing the pulverized and fragmented paste specimens for the microstructural examination .....	95
Figure 3.23	Thermal analyser used to study the mass stability in PMs and AABs.....	96
Figure 3.24	X-ray diffractometer used to study the mineralogy of PMs and AABs.....	97
Figure 3.25	Fourier transform infra-red spectrometer used to study the bond behaviour in PMs and AABs .....	97
Figure 3.26	Scanning electron microscope and energy dispersive spectroscopy used to study the morphology and elemental composition in PMs and AABs .....	99
Figure 3.27	Sputter coater used to vacuum dry and coat the PMs and AABs.....	99
Figure 4.1	Particle size distribution curve of the PMs .....	101
Figure 4.2	Morphology of SiMnF (left) and GGBFS (right) .....	103
Figure 4.3	X-ray diffractogram of PMs.....	106
Figure 4.4	FT-IR spectra of PMs.....	108
Figure 4.5	Effect of factors on compressive strength of AABs: (a) Factor A, (b) Factor B, (c) Factor C, (d) Factor D and (e) Factor E .....	111
Figure 4.6	Effect of factors and their levels on the 28-day compressive strength of AABs .....	112
Figure 4.7	The contribution of experimental factors on the compressive strength of AABs .....	117
Figure 4.8	Correlation between predicted values and experimental results .....	119
Figure 4.9	Setting times of AABs prepared by varying GGBFS/PMs ratio .....	121
Figure 4.10	Flow of AABs prepared by varying GGBFS/PMs ratio .....	122
Figure 4.11	Visual appearance of AABs exhibiting workability: discarded specimens with GGBFS content > 30% (left set) properly consolidated specimens with GGBFS content of < 30% (right set)	122

Figure 4.12	Compressive strength of AABs prepared by varying GGBFS/PMs ratio .....	123
Figure 4.13	X-ray diffractogram of GGBFS-free (M18) and optimum GGBFS-blended (M17) AABs.....	124
Figure 4.14	FT-IR spectra of GGBFS-free (M18) and optimum GGBFS-blended (M17) AABs.....	126
Figure 4.15	Thermogram of SiMnF-alone (M18) and optimum SiMnF-GGBFS blended (M17) AABs.....	128
Figure 4.16	Weight loss during heat treatment of SiMnF-alone (M18) and optimum SiMnF-GGBFS blended (M17) AABs.....	128
Figure 4.17	SEM images and EDS profiles of SiMnF-alone (M18) AAB .....	130
Figure 4.18	SEM images and EDS profiles of optimum SiMnF-GGBFS blended (M17) AAB .....	131
Figure 4.19	Setting times and flow of AABs: (a) AAs-free, Na <sub>2</sub> SiO <sub>3</sub> alone and NaOH alone, (b) varying NaOH molarity and (c) varying Na <sub>2</sub> SiO <sub>3</sub> /NaOH ratio .....	134
Figure 4.20	Compressive strength development of AABs: (a) AAs-free, Na <sub>2</sub> SiO <sub>3</sub> alone and NaOH alone, (b) varying NaOH molarity and (c) varying Na <sub>2</sub> SiO <sub>3</sub> /NaOH ratio.....	135
Figure 4.21	FT-IR spectra of AAs-free binder (M23), Na <sub>2</sub> SiO <sub>3</sub> -alone- (M24) and NaOH-alone- (M25) activated binders.....	136
Figure 4.22	SEM images of AAs-free binder (M23), Na <sub>2</sub> SiO <sub>3</sub> -alone- (M24) and NaOH-alone- (M25) activated binders.....	137
Figure 4.23	FT-IR spectra of AABs prepared with varying NaOH concentration .....	139
Figure 4.24	SEM images and EDS profile of AAB prepared with low 4 M NaOH concentration (M26) .....	141
Figure 4.25	SEM images and EDS profile of AAB prepared with mild 10 M NaOH concentration (M17) .....	141

Figure 4.26	SEM images and EDS profile of AAB prepared with high 16 M NaOH concentration (M29) .....	142
Figure 4.27	FT-IR spectra of AABs prepared with varying Na <sub>2</sub> SiO <sub>3</sub> to NaOH ratio .....	145
Figure 4.28	SEM images and EDS profile of AAB prepared with low Na <sub>2</sub> SiO <sub>3</sub> to NaOH ratio of 1 (M30) .....	146
Figure 4.29	SEM images and EDS profile of AAB prepared with mild Na <sub>2</sub> SiO <sub>3</sub> to NaOH ratio of 2.5 (M17) .....	147
Figure 4.30	SEM images and EDS profile of AAB prepared with high Na <sub>2</sub> SiO <sub>3</sub> to NaOH ratio of 3.5 (M34) .....	147
Figure 4.31	Compressive strength development in GGBFS-free (M35, M18 and M37) and SiMnF-GGBFS blended AABs (M36, M17 and M38) by varying curing methods.....	150
Figure 4.32	Compressive strength development in SiMnF-GGBFS blended AABs by varying curing period of 3 h (M39), 6 h (M40), 12 h (M41) and 24 h (M38) in comparison with water-cured (M36) and room-cured (M17) AABs.....	151
Figure 4.33	Compressive strength development in SiMnF-GGBFS blended AABs by varying curing temperature of 40 °C (M42) 60 °C (M40), 80 °C (M43) and 95 °C (M44) in comparison with water-cured (M36) and room-cured (M17) AABs.....	152
Figure 4.34	X-ray diffractogram of SiMnF-GGBFS blended AABs by varying curing period of 6h (M40) and 24 h (M38) in comparison with water-cured (M36) and room-cured (M17) AABs.....	156
Figure 4.35	X-ray diffractogram of SiMnF-GGBFS blended AABs by varying curing temperature of 60 °C (M40), 80 °C (M43) and 95 °C (M44) in comparison with water-cured (M36) and room-cured (M17) AABs.....	157
Figure 4.36	FT-IR spectra of SiMnF-GGBFS blended AABs by varying curing period of 3 h (M39), 6h (M40) and 24 h (M38) in comparison with water-cured (M36) and room-cured (M17) AABs.....	159

Figure 4.37	FT-IR spectra of SiMnF-GGBFS blended AABs by varying curing temperature of 60 °C (M40), 80 °C (M43) and 95 °C (M44) in comparison with water-cured (M36) and room-cured (M17) AABs .....	160
Figure 4.38	SEM images of SiMnF-GGBFS blended AABs by varying curing period of 3 h (M39), 6h (M40) and 24 h (M38) in comparison with water-cured (M36) and room-cured (M17) AABs.....	162
Figure 4.39	SEM images of SiMnF-GGBFS blended AABs by varying curing temperature of 60 °C (M40), 80 °C (M43) and 95 °C (M44) in comparison with water-cured (M36) and room-cured (M17) AABs .....	163
Figure 4.40	Compressive strength development of room-cured AABs before any exposure.....	167
Figure 4.41	Compressive strength of AABs immersed in pure H <sub>2</sub> O and 5% H <sub>2</sub> SO <sub>4aq</sub> .....	167
Figure 4.42	SEM images and EDS spectra of SiMnF-alone high-alkaline activated specimens exposed to pure H <sub>2</sub> O (M45) .....	170
Figure 4.43	SEM images and EDS spectra of SiMnF-GGBFS blended high-alkaline activated specimens exposed to pure H <sub>2</sub> O (M47) .....	170
Figure 4.44	SEM images and EDS spectra of SiMnF-GGBFS blended mild-alkaline activated specimens exposed to pure H <sub>2</sub> O (M49) .....	171
Figure 4.45	SEM images and EDS spectra of SiMnF-alone high-alkaline activated specimens exposed to 5% H <sub>2</sub> SO <sub>4aq</sub> (M46).....	172
Figure 4.46	SEM images and EDS spectra of SiMnF-GGBFS blended high-alkaline activated specimens exposed to 5% H <sub>2</sub> SO <sub>4aq</sub> (M48) .....	172
Figure 4.47	SEM images and EDS spectra of SiMnF-GGBFS blended mild-alkaline activated specimens exposed to 5% H <sub>2</sub> SO <sub>4aq</sub> (M50) .....	173
Figure 4.48	Typical micrograph of gypsum crystals and EDS spectrum formed in AABs immersed in 5% H <sub>2</sub> SO <sub>4aq</sub> .....	173
Figure 4.49	Appearance of typical AABs immersed in pure H <sub>2</sub> O.....	174

Figure 4.50	Appearance of AABs immersed in 5% $H_2SO_{4aq}$ after 10 and 20 weeks.....	174
Figure 4.51	Variation in pH of pure $H_2O$ and 5% $H_2SO_{4aq}$ solution upon exposure with AABs with time .....	176
Figure 4.52	Variation in mass of AABs immersed in pure $H_2O$ and 5% $H_2SO_{4aq}$ .....	178
Figure 4.53	X-ray diffractogram of SiMnF-alone high-alkaline (M45), SiMnF-GGBFS blended high-alkaline (M47) and SiMnF-GGBFS blended mild-alkaline (M49) activated specimens exposed to pure $H_2O$ .....	179
Figure 4.54	X-ray diffractogram of SiMnF-alone high-alkaline (M46), SiMnF-GGBFS blended high-alkaline (M48) and SiMnF-GGBFS blended mild-alkaline (M50) activated specimens exposed to 5% $H_2SO_{4aq}$ .	181
Figure 4.55	FT-IR spectra of SiMnF-alone high-alkaline (M45 and M46), SiMnF-GGBFS blended high-alkaline (M47 and M48) and SiMnF-GGBFS blended mild-alkaline (M49 and M50) activated specimens exposed to pure $H_2O$ and 5% $H_2SO_{4aq}$ .....	182
Figure 4.56	Compressive strength of AABs immersed in pure $H_2O$ and 5% $MgSO_{4aq}$ .....	188
Figure 4.57	SEM images and EDS spectra of SiMnF-alone high-alkaline activated specimens exposed to 5% $MgSO_{4aq}$ (M51) .....	190
Figure 4.58	SEM images and EDS spectra of SiMnF-GGBFS blended high-alkaline activated specimens exposed to 5% $MgSO_{4aq}$ (M52).....	190
Figure 4.59	SEM images and EDS spectra of SiMnF-GGBFS blended mild-alkaline activated specimens exposed to 5% $MgSO_{4aq}$ (M53).....	191
Figure 4.60	Appearance of AABs immersed in 5% $MgSO_{4aq}$ after 20 and 40 weeks.....	193
Figure 4.61	Variation in pH of pure $H_2O$ and 5% $MgSO_{4aq}$ solution upon exposure with AABs with time .....	194
Figure 4.62	Variation in mass of AABs immersed in pure $H_2O$ and 5% $MgSO_{4aq}$ .....	196

Figure 4.63	X-ray diffractogram of SiMnF-alone high-alkaline (M46), SiMnF-GGBFS blended high-alkaline (M48) and SiMnF-GGBFS blended mild-alkaline (M50) activated specimens exposed to 5% $MgSO_{4aq}$	198
Figure 4.64	FT-IR spectra of SiMnF-alone high-alkaline (M45 and M46), SiMnF-GGBFS blended high-alkaline (M47 and M48) and SiMnF-GGBFS blended mild-alkaline (M49 and M50) activated specimens exposed to pure $H_2O$ and $MgSO_{4aq}$	201
Figure 4.65	Compressive strength of AABs immersed in pure $H_2O$ and 5% $Na_2SO_{4aq}$	207
Figure 4.66	SEM images and EDS spectra of SiMnF-alone high alkaline specimens exposed to 5% $Na_2SO_{4aq}$ (M54)	209
Figure 4.67	SEM images and EDS spectra of SiMnF-GGBFS blended high-alkaline specimens exposed to 5% $Na_2SO_{4aq}$ (M55)	209
Figure 4.68	SEM images and EDS spectra of SiMnF-GGBFS blended mild-alkaline specimens exposed to 5% $Na_2SO_{4aq}$ (M56)	210
Figure 4.69	Appearance of AABs immersed in 5% $Na_2SO_{4aq}$ after 20 and 40 weeks	211
Figure 4.70	Variation in pH of pure $H_2O$ and 5% $Na_2SO_{4aq}$ solution upon exposure with AABs with time	212
Figure 4.71	Variation in mass of AABs immersed in pure $H_2O$ and 5% $Na_2SO_{4aq}$	214
Figure 4.72	X-ray diffractogram of SiMnF-alone high-alkaline (M46), SiMnF-GGBFS blended high-alkaline (M48) and SiMnF-GGBFS blended mild-alkaline (M50) activated specimens exposed to 5% $Na_2SO_{4aq}$	216

## LIST OF SYMBOLS

%	Percentage
°	Degree
°/min	Degrees per minute
°C	Degree Celsius
°2θ	Degree 2-theta
μm	Micro-meter or microns
σ	residual compressive strength in %
cm <sup>-1</sup>	Per centimeter
cm <sup>2</sup> /g	Square centimeter per gram
cm <sup>3</sup>	Cubic centimeter
cps	Counts per second
f <sub>c</sub>	Compressive strength in MPa
g	Gram
g/cm <sup>3</sup>	Gram per cubic centimeter
g/dm <sup>3</sup>	Gram per decimeter cube
Gt	Gigaton
h	Hour
ha	Hectare
kg/m <sup>3</sup>	Kilogram per cubic meter
km	Kilometer
kN	Kilo Newton
kN/sec	Kilo Newton per second
kV	Kilo Volts
L	Liter
M	Molarity, mole/L



Ms	Silica modulus (SiO <sub>2</sub> /Na <sub>2</sub> O)
m	Mass loss in %
m <sup>3</sup>	Cubic meter
m <sup>2</sup> /gr	Square meter per gram
m <sup>2</sup> /kg	Square meter per kilogram
m <sup>2</sup> /s	Square meter per second
mA	Milli ampere
min	Minute
mL	Milliliter
mm	Millimeter
MMT	Million metric ton
mol./L	Moles per liter
MPa	Mega Pascal
Mt	Megaton
N	Newton
ng/m <sup>3</sup>	Nanogram per cubic meter
nm	Nano-meter
P	Pascal
pH	Power of hydrogen
ppm	Parts per million
rpm	Rotations per minute
s	Second
s.g.	Specific gravity
V	Volt

## LIST OF ABBREVIATIONS

AA	Alkaline activators
AAB	Alkali-activated binder (a general term used for alkali-activated paste and mortar)
AAM	Alkali-activated mortar
AAC	Alkali-activated concrete
AAS	Alkali-activated slag
ANOVA	Analysis of variance
ASTM	American Society for Testing and Materials
CAA	Combine alkaline activators
CAS #	Chemical Abstracts Service number
C-A-S-H	Calcium-Alumina-Silicate-Hydrate
C-S-H	Calcium Silicate Hydrate
C/N-A-S-H	Calcium/Sodium-Alumina Silicate Hydrate
C-Mn-S-H	Calcium Manganese Silicate Hydrate
DOE	Design of experiments
EDS	Energy Dispersive Spectroscopy
FA	Fly ash
FAG	Fine aggregate
FeMn	Ferromanganese
FT-IR	Fourier Transform Infra-Red
FW	Free water
GGBFS	Ground granulated blast furnace slag
GHG	Green House Gas
IMnI	International Manganese Institute
I.S.T.	Initial setting time
F.S.T.	Final setting time
K-A-S-H	Potassium Aluminosilicate Hydrate
LOI	Loss on Ignition
M #	Mix number (i.e., M1 to M56)
Mn-S-H	Manganese silicate hydrate
MK	Metakaolin
N-A-S-H	Sodium-Alumina-Silicate-Hydrate

NH	Sodium hydroxide
NP	Natural pozzolan
NS	Sodium silicate
OPC	Ordinary Portland cement
PDF #	Powder Diffraction File number
PM	Precursor material
PMs	Precursor materials (i.e., SiMnF and GGBFS)
POFA	Palm oil fuel ash
S	Spectrum
SAI	Strength activity index
SCMs	Supplementary cementitious materials
SEM	Scanning Electron Microscope
SF	Silica fume
SiMn	Silico-manganese
SiMnF	Silico-manganese fume
SiMnS	Silico-manganese slag
S/N	Signal to noise ratio
TG	Thermogravimetric
TGA	Thermogravimetric analysis
TL	Total liquid (sum of AAs and FW)
TM	Taguchi Method
UN	United nations
UNEP	United Nations Environment Programme
XRD	X-ray Diffraction
XRF	X-Ray Fluorescence

# **PEMBANGUNAN PENGIKAT TERAKTIF ALKALI MENGGUNAKAN WASAP SILIKA-MANGAN DAN JERMANG RELAU BAGAS**

## **ABSTRAK**

Kesan negatif peningkatan penghasilan wasap silika-mangan (SiMnF), kira-kira 100-150 kg untuk setiap tan aloi SiMn yang dihasilkan dan peningkatan jejak karbon disebabkan oleh pengeluaran simen Portland biasa (OPC) menunjukkan perlunya kajian ini. Ini diperlukan untuk meningkatkan kesihatan awam, meminimumkan penjanaan sisa pepejal, mengurangkan pemanasan global dan mengembangkan bahan pembinaan alternatif yang menjimatkan kos untuk infrastruktur kejuruteraan awam. Tesis ini memaparkan penggunaan teknologi pengikat teraktif alkali untuk mengurangkan cabaran yang berkaitan dengan industri konkrit dan lain-lain yang berkaitan. Ini membawa kepada pembangunan mortar teraktif alkali (AAMs) baharu yang mampan menggunakan kandungan wasap silika-mangan yang tinggi (SiMnF) dan jermang relau bagas (GGBFS) sebagai bahan prekursor (PMs) bersama dengan  $\text{NaOH}_{\text{aq}}$  (NH) dan  $\text{Na}_2\text{SiO}_{3\text{aq}}$  (NS) sebagai pengaktif alkali (AAs). Pengoptimuman campuran mortar dicapai dengan menggunakan tatasusunan ortogonal L16 berdasarkan kaedah Taguchi (TM). Parameter campuran yang dikaji adalah nisbah GGBFS / PMs (0-0.5), nisbah pasir / PMs (1.5-2.4), kepekatan NH (0-16M), nisbah NS / NH (0-3.5), modulus silika (0-3.4) dan nisbah AAs / PMs (0.5-0.53). Pengaruh kaedah pengawetan, iaitu pengawetan suhu bilik, pengawetan lembap, dan pengawetan haba (selama 3-24 jam antara 25-95°C) dan prestasi ketahanan di bawah pendedahan persekitaran asid dan sulfat juga dikaji. Ciri-ciri segar dan kekuatan mekanikal telah dinilai, manakala kajian analitik seperti kestabilan jisim, ciri ikatan, sifat produk yang terbentuk dan morfologi struktur mikro,

masing-masing telah dijalankan menggunakan analisis termogravimetrik (TG), analisis FT-IR, analisis difraksi sinar-X (XRD), dan mikroskop elektron imbasan (SEM) ditambah spektroskopi penyebaran tenaga (EDS). Campuran mortar optimum terdiri daripada nisbah SiMnF:GGBFS, pasir/PMs,  $\text{Na}_2\text{SiO}_{3\text{aq}}/10\text{M-NaOH}_{\text{aq}}$  dan AAs/PMs 70:30 wt.%, 1.5, 2.5 dan 0.5, di mana nisbah  $\text{SiO}_2/\text{Na}_2\text{O}$ ,  $\text{H}_2\text{O}/\text{Na}_2\text{O}$  dan  $\text{H}_2\text{O}/\text{SiO}_2$  masing-masing adalah 1.61, 17.33 dan 10.77. Gabungan ini menghasilkan kekuatan mampatan 3-, 7- dan 28 hari, masing-masing 22.5, 29.7 dan 44.5 MPa pada pengawetan bilik, manakala pengawetan haba selama 6 jam pada  $60^\circ\text{C}$  bermanfaat untuk mencapai kekuatan tertinggi dalam 3 -hari. Antara sebatian yang menonjol yang menentukan struktur mikro AAMs yang dibangunkan adalah fasa stratlingite / gehlenite hydrate (C-A-S-H), nchwanningite / glaucochroite (C-Mn-S-H), dan kalium feldspar (K-A-S-H). Pendedahan produk terhadap serangan asid menyebabkan kemerosotan lebih cepat dengan penyahkalsifikasi dan pembentukan gipsium dengan ikatan S-O dan pembentukan karbonasi sebagai hasil kereaktifan kapur dengan  $\text{CO}_2$  atmosfera. Pendedahan kepada  $\text{MgSO}_{4\text{aq}}$  menyebabkan kemerosotan yang lebih ketara yang membawa kepada pengelupasan spesimen ekor daripada pembentukan kristal gipsium dan brucite dibandingkan dengan  $\text{Na}_2\text{SO}_{4\text{aq}}$  di mana kestabilan dibantu oleh sebatian berasaskan kuarza. Adalah dijangkakan bahawa hasil yang diperoleh dari AAMs baharu yang dibangunkan akan bermanfaat dalam memahami tingkah laku dan sebagai inisiatif terhadap aplikasi praktikal bahan disamping mencapai kelebihan dari aspek ekonomi, ekologi dan teknikal.

# **DEVELOPMENT OF ALKALI-ACTIVATED BINDER UTILIZING SILICO-MANGANESE FUME AND BLAST-FURNACE SLAG**

## **ABSTRACT**

The negative impacts of proliferation of silico-manganese fume (SiMnF) of about 100-150 kg per tonnage of SiMn alloy produced and increase in the carbon footprint due to production of ordinary Portland cement (OPC) premised the need for this study. This is necessary to enhance public health, minimize the solid waste generation, reduce global warming and develop alternative cost-efficient construction materials for civil engineering infrastructures. This thesis addresses the use of alkali-activated binding technology to mitigate the challenges associated with the concrete and other industries. This led to the development of novel and sustainable alkali-activated mortars (AAMs) using high level of silico-manganese fume (SiMnF) and ground granulated blast furnace slag (GGBFS) as precursor materials (PMs) together with  $\text{NaOH}_{\text{aq}}$  (NH) and  $\text{Na}_2\text{SiO}_{3\text{aq}}$  (NS) as the alkaline activators (AAs). The optimization of mixes was achieved using L16 orthogonal array based on the Taguchi method (TM). The mix parameters studied were GGBFS/PMs (0-0.5), sand/PMs (1.5-2.4), NH concentration (0-16M), NS/NH ratio (0-3.5), silica modulus (0-3.4) and AAs/PMs (0.5-0.53). The influence of curing methods, namely room-, moist-, and heat-curing (for 3-24 h between 25-95 °C) and durability performance under the exposure to acid and sulphate environments were also studied. Fresh properties and mechanical strength were evaluated, while analytical studies, such as mass stability, bond characteristics, nature of the products formed and morphology of the microstructures were undertaken using thermogravimetric (TG) analysis, FT-IR analysis, X-ray diffraction (XRD) analysis, and scanning electron microscopy (SEM)

plus energy dispersive spectroscopy (EDS), respectively. The optimum mortar mix consisted of SiMnF:GGBFS, sand/PMs,  $\text{Na}_2\text{SiO}_{3\text{aq}}$ /10M- $\text{NaOH}_{\text{aq}}$  and AAs/PMs ratios of 70:30 wt.%, 1.5, 2.5 and 0.5 such that the  $\text{SiO}_2/\text{Na}_2\text{O}$ ,  $\text{H}_2\text{O}/\text{Na}_2\text{O}$  and  $\text{H}_2\text{O}/\text{SiO}_2$  ratios were 1.61, 17.33 and 10.77, respectively. This combination yielded a 3-, 7- and 28-day compressive strength of 22.5, 29.7 and 44.5 MPa, respectively at room-curing, whereas the heat-curing for 6 h at 60 °C was beneficial for attaining the highest strength within 3-days. Among the prominent compounds that defined the microstructure of the developed AAMs were stratlingite/gehlenite hydrate (C-A-S-H), nchwangingite/glaucocroite (C-Mn-S-H), and potassium feldspar (K-A-S-H) phases. Exposing the product to acid attack caused faster deterioration by decalcification and formation of gypsum with S-O bonds and formation of carbonation as a result of reactivity of lime with atmospheric  $\text{CO}_2$ . Exposure to  $\text{MgSO}_{4\text{aq}}$  caused more deterioration leading to spalling of specimens due to formation of gypsum and brucite crystals in comparison with  $\text{Na}_2\text{SO}_{4\text{aq}}$  where the stability was aided by quartz-based compound. It is envisaged that the results obtained from the novel AAMs would be beneficial in understanding the behaviour and an initiative towards practical application of the materials beside attaining economic, ecological and technical advantages.

# CHAPTER 1

## INTRODUCTION

### 1.1 Background to the study

The ecosystem of the planet Earth is encountering hostile changes due to global warming such as increased melting of glacier coupled with rise in sea levels, noticeable shifts in rain and snow fall patterns, huge desertification, severe drought and floods, stronger hurricanes and cyclones. These changes are expected as human beings are adding the heat-trapping greenhouse gases (GHGs) to the atmosphere. The fifth assessment report of the Intergovernmental Panel on Climate Change confirmed that the GHGs emissions is the primary contributor of global warming since the mid-20<sup>th</sup> century (Stocker et al., 2013). It is estimated that the main gas contributing to GHGs is carbon dioxide (CO<sub>2</sub>) = 76%, followed by methane (CH<sub>4</sub>) = 16%, nitrous oxide (N<sub>2</sub>O) = 6% and F-gases = 2% (Intergovernmental Panel on Climate Change, 2014). As per the consensus of Paris convention of UN, it was agreed to minimize the total world CO<sub>2</sub> emissions to below 50 Gt by 2020 in order to overcome the climate change and to keep the global warming temperature below 2 °C (United Nations, 2017). The punitive environmental legislations for different industries were imposed by the global community to limit the anthropogenic GHGs emissions by adopting sustainable and innovative measures. According to the international energy agency (IEA), electricity generation, construction sector and transportation are the top three contributors of GHGs emissions (International Energy Agency (IEA), 2019). Among them construction sector consumes approximately 40% of the world's energy, 30% of raw materials, 25% of water, 25% of solid waste, 12% of land which corresponds to 33% of the global GHG emissions, according to the report of United Nations Environment Programme (UNEP) (UNEP, 2009). It is well-known that cement and concrete are the



largest man-made elements on the Earth such that the cement industry is one of the world largest industries in contributing carbon emissions in the world. There are several environmental problems posed by cement-based binders which tend to be alarming due to worldly boom of construction. For example, the concrete consumption in the Burj Khalifah - the world's tallest structure was around 250,000 m<sup>3</sup> (Subramanian, 2010). Further, the demand for ordinary Portland cement (OPC) is continuously escalating with time and it is expected to reach to 5.9 billion tons by 2020 leading to 4.8 billion tons of CO<sub>2</sub> emissions (Singh and Middendorf, 2020). The worldly consumption of concrete per capita is estimated to be around 1 m<sup>3</sup> (Gartner, 2004) which is predicted to grow four-folds by 2050 compared to that in 1990 attributed to continuous increase in rate of the population and infrastructural demand. The World Business Council for Sustainable Development (WBCSD) reported that the production of each ton of OPC releases CO<sub>2</sub> in the range of 0.73-0.99 tons (WBCSD, 2011). This corresponds to 5 - 7% of global anthropogenic CO<sub>2</sub> emission in to the atmosphere (Worrell et al., 2001). It is estimated that considering constant production rate and process of OPC, the amount of CO<sub>2</sub> emissions will be multiplied by 5 fold in 2050 as compared to that registered in 1990 (Imbabi et al., 2012). Additionally, the cement industry consumes 120 kWh of energy per ton of OPC production which accounts for 10 to 15% of the total world industrial energy (Ali et al., 2011; Madloul et al., 2011). According to the European Cement Association (CEMBUREAU, 2011) the fuel firing requirement for every ton of cement production is around 60 – 130 kg. In order to alleviate the undesirable effects of OPC production, following four options are often proposed (Mokhtar and Nasooti, 2020; Singh and Middendorf, 2020): a) energy efficient technologies for energy conservation; b) incorporating alternative waste fuels and recovering energy measures; c) equipping CO<sub>2</sub> emission reduction

systems such as carbon capture and storage; and d) modifying product and feedstock either by producing low alkali and limestone cements or by reducing the clinker-to-cement ratio using supplementary cementitious materials (SCMs) or adopting alkali-activated technology.

There are several environmental problems also posed by other industries which generate huge volumes of solid waste. For instance, the common manufacturing industrial waste includes fly ash (FA) / pulverized fly ash (PFA) / Super pozz (SP), ground granulated blast furnace slag (GGBFS), silica fume (SF) / micro-silica (MS) and silico-manganese fume (SiMnF) / silico-manganese slag (SiMnS) which are the by-products of coal power plants, iron/steel industry, silicon industry and ferroalloy industry, respectively. The agricultural industry is responsible for generating the waste from date palm, palm oil, rice husk, sugarcane bagasse, wheat straw, coconut coir, corncob, elephant grass, bamboo, olive and other trees. The generation of red mud from the alumina production and existence of other natural minerals like metakaolin and natural pozzolan also account for huge reserves. In this vein, extensive research has been carried out hitherto to recycle several types of agricultural wastes (Aprianti et al., 2015), industrial by-products (Buchwald and Schulz, 2005) and natural resources (Robayo-Salazar and de Gutiérrez, 2018) as construction materials.

Cement and concrete technologists are continuously striving to adopt sustainable construction practices that can mitigate the greenhouse gas emissions, lower the energy consumption, conserve natural resources and recycle the solid wastes. Among various options available, evolution of geopolymer (Davidovits, 1991) or alkali-activated binder (AAB) (Provis et al., 2015) technology has enticed the researchers by virtue of its value-added and countervailing sustainability solutions enabling clinker-free and solid waste-based construction. AAB has two main

components; alkaline activators (AAs) like sodium/potassium-based hydroxide and silicate ( $\text{Na/K-OH}$  and  $\text{Na}_2/\text{K}_2\text{-SiO}_3$ ) and precursor materials (PMs) like aluminosilicate-rich [ $(\text{AlO}_4)^{5-}$  and  $(\text{SiO}_4)^{4-}$ ] (Provis, 2014). AAB is an inorganic polymer coined as a result of the polycondensation reaction between activators and individual tetrahedral in PMs when cured at a suitable temperature (Provis, 2014). Generally, a 3D amorphous structure of N-A-S-H ( $\text{Na}_2\text{O-Al}_2\text{O}_3\text{-SiO}_2\text{-H}_2\text{O}$ ) gel is the primary reaction product in low Ca-based aluminosilicate precursors, whereas C-(N)-A-S-H and C-A-S-H ( $\text{CaO-Al}_2\text{O}_3\text{-SiO}_2\text{-H}_2\text{O}$ ) are the main reaction products in high Ca-based AABs, unlike the C-S-H gel formed during the hydration of OPC (Provis et al., 2015). It is estimated that the production of AAB has lower environmental impacts, such as emission of 80% lower  $\text{CO}_2$  than OPC. It is reported that leaching of toxic elements can be minimized through the development of AAB (Vu and Gowripalan, 2018). Recent reviews on AAB indicated that numerous agro-industrial and other natural minerals have been successfully valorised as PMs for the AAB production exhibiting excellent engineering and durability characteristics (Elahi et al., 2020; Garg et al., 2020; Zhang et al., 2020). However, the properties of some unidentified wastes and their synthesis at ambient temperature condition is yet to be explored as a construction product and to extend their applications in cast in-situ applications.

## 1.2 Problem statement

Silico-manganese fume (SiMnF) and silico-manganese slag (SiMnS) are the by-products of manufacturing silico-manganese (SiMn) alloy at ferroalloy industry. SiMn alloy is produced by the carbo-thermal reduction process of oxide ores in an electric arc furnace at  $1500\text{ }^\circ\text{C}$  and utilized in steel making as deoxidizing agent. According to International Manganese Institute (IMnI), production of one ton of SiMn

alloy generates 15% Mn dust/fume which contributes approximately 15 MMT of global SiMn waste (IMnI, 2018). It was reported in an earlier study (Nath and Kumar, 2016) that SiMnS possesses similar characteristics as ground granulated blast furnace slag (GGBFS). However, their composition could vary widely depending on the origin of raw materials used in SiMn alloy production, such as Mn ore, quartz, limestone and reductants (coke/coal).

The reactivity of SiMn wastes is considered very low due to the high concentration of Mn, Si and K as well as low quantity of Ca. Previous studies on SiMn waste indicated that it can be activated through mechanical, thermal and/or chemical processes to improve its reactivity. Studies between 1999 and 2016 indicated that partial substitution of Portland cement by SiMnS to the level of 50% could be possible (Péra et al., 1999; Rai et al., 2002; Frias et al., 2005, 2006; Frias and Rodríguez, 2008; Frías et al., 2009; Allahverdi and Ahmadnezhad, 2014; Nath and Kumar, 2016). Other researchers evaluated the effect of milling of SiMnS (Allahverdi and Ahmadnezhad, 2014; Kumar et al., 2013), slag cooling and curing methods on hydraulicity or reactivity and strength development of binder (Choi et al., 2017; Navarro et al., 2017; Rai et al., 2002). Few studies focused on the development of alkali-activated binder (AAB) by using SiMnS alone (Kumar et al., 2013; Navarro et al., 2017), SiMnS blended with fly ash (Nath and Kumar, 2018, 2017) and SiMnS blended GGBFS (high volume GGBFS = 90%) (Criado et al., 2018). It was reported that the mechanical strength of SiMnS-based AAB tends to increase in the presence of reactive CaO due to dual formation of C-A-S-H and N/C-A-S-H gel (Nath and Kumar, 2017). Blending Mn-rich SiMnS with GGBFS also decreased the tendency of reinforcement corrosion in AAB (Criado et al., 2018). Some other products that defined SiMn waste include hydrated calcium manganese (C-Mn-H) (Frias et al., 2006) and hydrated manganese

silicate (Mn-S-H) (Najamuddin et al., 2019) in the presence of lime and alkaline media, respectively.

Ground granulated blast furnace slag (GGBFS) is the by-product of steel industry whose annual world production accounts up to 370 million ton and it is often used as a binder in the construction industry due to the existence of high and amorphous concentrations of Ca, Si and Al (Aydin and Baradan, 2014). Under alkaline media, GGBFS exhibits hydraulic binding and pozzolanic characteristics (Puertas et al., 2000). Unlike fly ash-based AAB that contains excessive crystalline compounds and requires heat-curing (40 – 85 °C) for activation, GGBFS-based binders undergo accelerated reaction under the condition of room temperature curing (Puertas et al., 2000). Several studies (Puertas et al., 2000; Rashad, 2013) affirmed that the presence of extra Ca in the GGBFS-based AAB improves its mechanical and microstructural properties. The excellent synergy of GGBFS with several supplementary cementitious materials is proven during alkaline-activation which is attributed to the virtue of formation of multiple hydration products, such as C-S-H, C-A-S-H and C-(Na)-S-H (Fernández-Jiménez et al., 2003), zeolites (natrolite and gismondine) (Zhang et al., 2008), hydrotalcite- (Liu et al., 2018) and AFm-type phases (Bonk et al., 2003).

### **1.3 Significance of research**

The proliferation of SiMnF calls for its usage in large quantities together with others with hydraulic property, such as GGBFS. This is possible by means of alkali-activation technology. **Figure 1.1** compares the number of publications related to the use of SiMnF, SiMnS, palm oil fuel ash (POFA), natural pozzolan (NP), metakaolin (MK), ground granulated blast-furnace slag (GGBFS) and fly ash (FA) as precursors in the development of AAB.

According to the key words searched on Scopus, number of publications involving SiMnS- and SiMnF-based alkali-activated materials are researched only 2 and 1 times, respectively. It indicated that SiMn waste was overlooked in the literature.

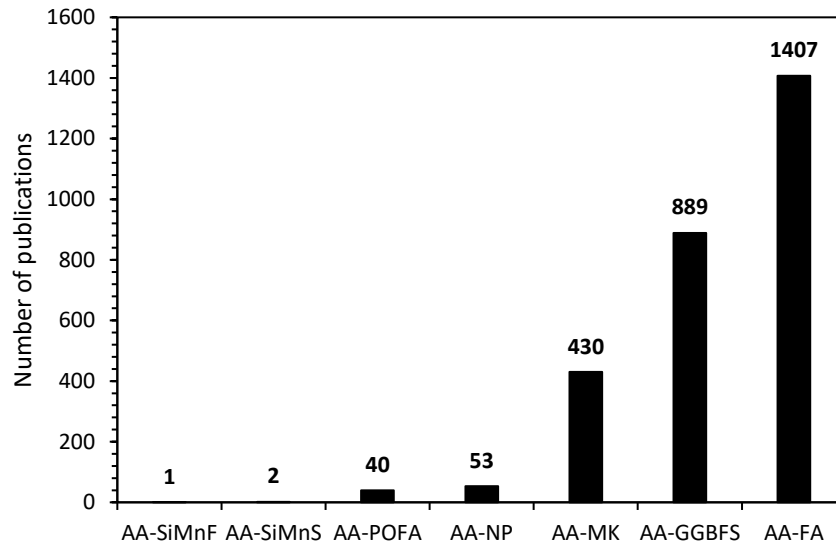


Figure 1.1 Number of publications on alkali-activated materials [Courtesy: scopus.com, last accessed on 10-10-2020]

Hence, to fulfil the knowledge gap and to promote the application of SiMnF as a promising precursor, a detailed investigation was undertaken. GGBFS was partially blended with SiMnF to enhance its reactivity. The raw precursors were characterized thoroughly using advanced analytical tests to predict their role in the development of AAB. Several mix parameters of AAB were designed using optimization techniques. The optimized mix proportions, such as precursor content, alkali concentration, activator dosage of the experimental program was investigated in detail. The reaction kinetics of the developed binders particularly the role of abundance of Mn, K and Si present in the SiMnF and their synergy with the Ca and Al species present in the GGBFS was tried to be understood beside the impact of alkaline activators in the synthesis of AAB. The fresh, mechanical and microstructural characteristics of SiMnF-based AAB was established. The influence of thermal curing, such as curing

period and curing temperature was explored in order to extend the applicability of the PMs in pre-stress, pre-cast and cast in-situ applications to attain cut-short in energy, early formwork stripping and accelerating the construction pace. The durability of SiMnF-based AAB was investigated under the long-term exposure of acid- and sulphate-environments. It is hypothesized that the synergistic-effect of both PMs may complement each other through alkali-activation yielding good structural characteristics of the binder. It is also expected that the developed SiMnF-based AAB will provide promising alternative solution by eliminating the main landfilling problems which creates odour, noise, space scarcity and taxation associated with industrial waste, reduce the risk of land sliding caused by stockpiling the waste, minimize the health hazards pertaining to SiMn waste exposure, lower environmental impact compared to the production of currently unrivalled OPC. It is envisaged that the results obtained from the proposed binder would be beneficial in understanding the behaviour and practical application of the novel binder. It is also expected that the developed AAB will grossly provide economic, ecological and technical advantages.

#### **1.4 Objectives of research**

The primary aim of this research was to develop alkali-activated binder (AAB) utilizing novel silico-manganese fume (SiMnF) as main precursor material (PM) in synergy with the ground granulated blast furnace slag (GGBFS). The rationale of admixing GGBFS was to maximize the reactivity of Mn, K and Si rich SiMnF which will potentially enable the AAB to be used in both cast-in-place and pre-cast applications beside enhancing the strength. The fresh, mechanical, durability and microstructural characteristics of the developed AABs were also assessed. The following are the objectives of this research;

1. To characterize the raw precursor materials
2. To establish the optimum mix and curing parameters of the SiMnF-based AABs.
3. To evaluate the durability or chemical resistance of the developed AABs under acid and sulphate environments.

### **1.5 Scope of the research**

The scope of this research encompasses four major components:

1. Firstly, SiMnF and GGBFS were procured from the local industrial plants and characterized by colour, shape, particle size distribution, surface area, specific gravity, oxide chemical composition, loss on ignition, mineralogy, bond characteristics, morphology and elemental analysis.
2. Secondly, trial alkali-activated mixtures were prepared as suggested by the Taguchi method of experimental design by varying ratio of GGBFS to PMs in the range of 0 to 45, sand to PMs ratio in the range of 1.5 to 2.4, the molarity of NaOH in the range of 4 to 10 M, the ratio of Na<sub>2</sub>SiO<sub>3</sub> to NaOH in the range of 2 to 3.5 and ratio of AAs to PMs in the range of 1.5 to 2.4. The strength data was statistically analysed followed by the experimental validation.
3. Thirdly, based on the outcomes of the trial mixture, the role of PMs (GGBFS/GGBFS+SiMnF = 0 to 0.5), effect of alkali concentration (NaOH = 0 – 16 M) and activator dosage (Na<sub>2</sub>SiO<sub>3</sub> to NaOH = 0 – 3.5) and influence of curing method, namely ponding, ambient and heat curing period and temperature. The heat curing period was optimized within 3 to 24 h at 60 °C and the curing temperature was optimized within 25 to 95 °C at 6 h. The representative fresh and mechanical properties were evaluated and



complimented with the mineralogy, bond characteristics, morphology and elemental analysis.

4. Lastly, the performance of the room-cured AABs prepared by varying NaOH concentration (4 and 10 M) and GGBFS content (0 and 30%) was assessed by determining its resistance to sulfuric acid (5% H<sub>2</sub>SO<sub>4</sub> up to 20 weeks), sodium sulphate (5% Na<sub>2</sub>SO<sub>4</sub> up to 40 weeks) and magnesium sulphate (5% MgSO<sub>4</sub> up to 40 weeks) attacks. The deterioration mechanism was monitored by visual inspection, variation in alkalinity, mass loss, compressive strength retention and microstructural changes.

The followings some limitations of this research:

1. The research is limited to the application of SiMnF-alone and SiMnF-GGBFS blended alkali-activated binder in paste and mortar but not extended to concrete.
2. The research explores the optimization of the range of certain mixture and curing parameters on fresh and strength characteristics complimented with the microstructural analysis of the product, however, it is not extended to the structural performance of the products in a structural element such as slab, beams or columns.
3. The research explored the resistance of developed binders under certain chemical attacks and the deterioration mechanism associated with them.

## **1.6 Organization of the thesis**

The thesis is divided into the five main chapters followed by the references section:

- Chapter one: An overview of introduction and motivation of the research work, significance and limitations of research, aims and objectives of the research, scope and organization of the thesis.
- Chapter two: Comprehensive literature review and recent advances in the area of research.
- Chapter three: Techniques used to design and optimize the experimental program, details of experimental work performed in order to achieve the research objectives.
- Chapter four: Results and discussion for optimization of mix parameters and in-depth assessment of fresh, strength, durability and microstructural properties of the developed mortar and paste mixes.
- Chapter five: Conclusions and recommendations and suggestions for future extension of the work.

## CHAPTER 2

### LITERATURE REVIEW

#### 2.1 Preamble

Socio-scientific obligations have prompted the cement and concrete technologists to utilize industrial by-products as a substitute for cement to mitigate the alarming threats associated with Portland cement production. The threats include depletion of natural resources, high CO<sub>2</sub> emissions, intensive energy consumption and other industrial challenges such as landfill volume extensions, waste generation taxation, odour, and pollution. In this pursuit, researchers have explored some alternative binders, such as calcium sulfo-aluminate cement (Ali et al., 1994), magnesium-based cement (Yang et al., 2017) and alkali-activated binders (AABs) (Deventer et al., 2010). Among them alkali-activated technology is known as one of the viable alternative options having the dual advantages of producing clinker-free and solid waste-based green construction products.

Alkali-activated binder (AAB) is formed when alkaline activators like aqueous NaOH and Na<sub>2</sub>SiO<sub>3</sub> react with aluminosilicate or calcareous based materials (Davidovits et al., 1990). These precursor materials may originate from agricultural waste, building materials, chemical, glass, metallurgical and mine industries. Generally, C-A-S-H and C-(N)-A-S-H are the main reaction products in high Ca-based AABs, whereas N-A-S-H gel is the primary reaction product in low Ca-based aluminosilicate precursors. Recent reviews on the AAB reported that the synthesized AAB exhibits excellent fresh, engineering and durability properties (Elahi et al., 2020; Garg et al., 2020; Zhang et al., 2020).

Nonetheless, the performance of the developed AAB differs considerably due to various factors, such as composition of the precursor materials (PMs) and alkaline

activators as well as the curing practices. Therefore, it is crucial to comprehend the reaction kinetics involved in the synthesis of any AAB and to assess its engineering and durability characteristics in order to formulate the optimum mix proportion of an AAB for the desired applications. Hitherto, enormous researches have been conducted in the last few decades incorporating several PMs and alkaline activators for the synthesis of AAB whose focus was the evaluation of the role played by the composition of the binder and development of the microstructure (Mehta and Siddique, 2016). However, the application of the developed AAB was limited to few in the field. This is possibly due to the fact that there exist some unresolved issues in the mass-scale production and cast in-situ applications for the infrastructural developments.

A classical review of the literature and recent advancement in the production of AAB utilizing various PMs is presented in the subsequent sections including but not limited to historical background, basic concepts of synthesis of AAB, factors influencing the properties of AAB, engineering and durability characteristics of AAB. Based on the outcomes of the existing studies, the major difficulties in the technology are highlighted and knowledge gaps are identified. Consequently, the objectives of this research mainly to undertake the identification and characterization of the novel solid waste which can potentially be immobilized in the development of AAB leading to acceptable properties for construction applications.

## **2.2 Cement production and associated problems**

Cement has been registered as the largest man-made element and second most consumed substance on the Earth after the essential requirement of water. Cement has essential role of imparting hydraulic binding property in concrete and by virtue of its properties, basic necessities of infrastructure to the iconic structures and luxurious life

style has been possible for human. Since the discovery of cement in England by Joseph Aspdin during the 19<sup>th</sup> century as well as with the increase in the rate of population, the life without cement can hardly be imagined. It is estimated that the present worldly demand of cement is 4.6 billion tons which is expected to grow about 6 billion tons by the end of 2050 (Scrivener et al., 2018). They also correlated the worldwide amount of steel and cement produced with the growth of population, as illustrated in **Figure 2.1**.

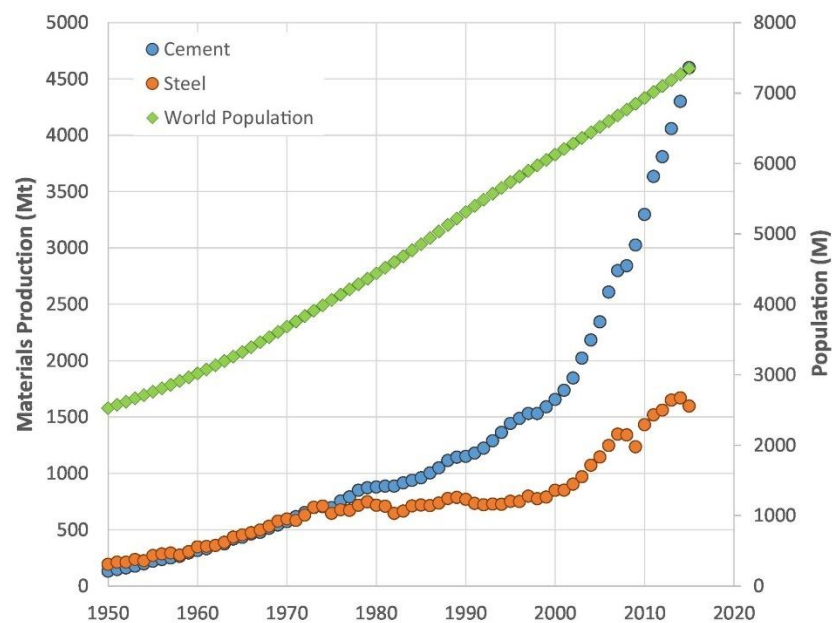


Figure 2.1 Comparison of cement and steel production with the population [Courtesy: Scrivener et al. (2018)]

The worldwide boom of construction is posing an alarming threat because the production process of cement is highly energy-intensive. Cement production involves three main stages such as preparing raw material, clinker production and finally grinding of cement, as detailed in **Figure 2.2**. Among these steps, 70 to 80% of the total energy is consumed during clinker making (Boesch et al., 2009). It is estimated that production of 1 ton of clinker consumes 4427 MJ of the energy which corresponds to 2% of global energy and 5% of the global industrial energy (Boesch et al., 2009).

Thus, the energy requirement constitutes 20 to 40% of the total cost of the cement manufacturing (Singh and Subramaniam, 2019).

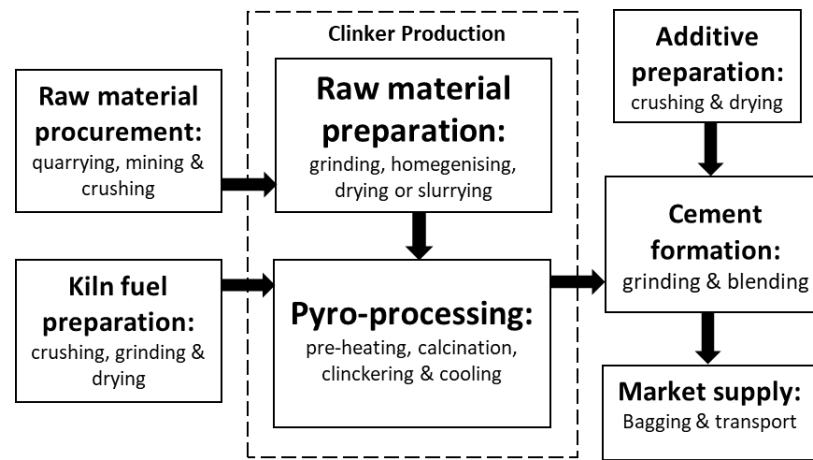


Figure 2.2 Cement manufacturing process  
[Adapted: Ruth (2000)]

Due to highly energy-intensive processes involved in the cement production, it is also a big contributor to the global warming. It is reported that about 3% of the global greenhouse gasses (GHGs) and 7% of the CO<sub>2</sub> emissions are associated with the cement industry. According to Nidheesh and Kumar (2019), the production of each ton of cement discharges 730 to 990 kg of CO<sub>2</sub> in to the atmosphere such that contribution of GHGs from process, fossil fuel, electricity and transportation accounts 50%, 40%, 5% and 5%, respectively, as shown in Fig 2.3. It is predicted that by 2020 there is likelihood of triggering the threshold global warming danger-zone of 2 °C to rise up to 75% if the CO<sub>2</sub> discharge exceeds 50 Gt (Meinshausen et al., 2009).

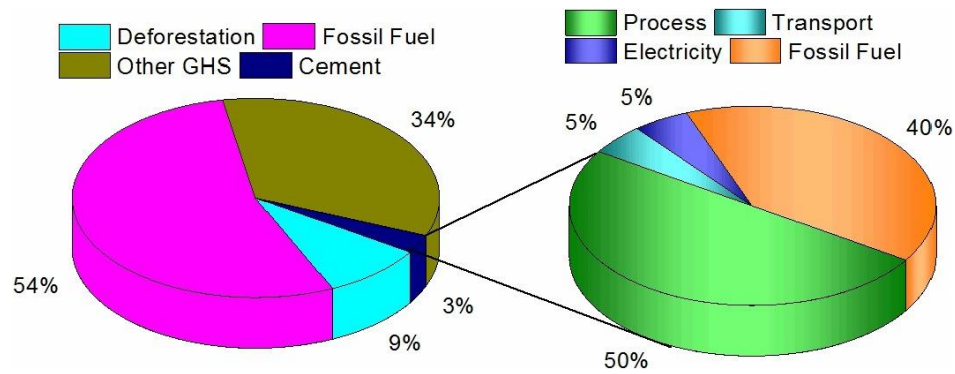


Figure 2.3 Greenhouse gases (GHGs) emissions from cement production [Courtesy: Nidheesh and Kumar (2019)]

An overview of environmental sustainability in cement production concluded that the major challenges associated with the cement production can be alleviated by the replacement of raw materials and fuel technology. For instance, the use of blended cements and adopting the co-processing methods (Nidheesh and Kumar, 2019). Moreover, the OPC concrete poses certain durability problems when the structure is subjected to chloride, sulphate and acid environments. A partial replacement of SCMs to OPC also offer enhancement of durability characteristics.

### 2.3 Solid wastes generation and associated problems

Solid wastes are broadly categorized into two types: industrial or agricultural waste and municipal household garbage. Usually, these wastes are either bunt in open air, disposed to landfill or stockpiled without being recycled in developing countries.

#### 2.3.1 Hazards of exposure to solid wastes

Open field burning is considered as inexpensive approach to enhance crop rotation but several environmental and health problems are associated with it due to fine firing emissions such as soot, particulate matter (PM), carbon monoxide (CO), methane (CH<sub>4</sub>), polycyclic aromatic hydrocarbons (PAH), polychlorinated dibenzo-p-dioxins (PDD), and polychlorinated dibenzofurans (PCD), elemental carbon (EC) and

organic carbon (OC) that disperse in surrounding air and when people victim by unsuspectingly inhalation cause acute effects with delicate respiratory disease (Estrellan and Iino, 2010). Similarly, industrial discharges may also consist of hazardous characteristics such as toxicity, corrosiveness, flammable or combustible, chemically reactive and infectious (He et al., 2016).

### **2.3.2 Landfilling and stockpiling problems**

Landfilling causes space scarcity issues as well as problems of land sliding. Therefore, landfill taxation laws have been implemented in several countries to mitigate the landfill volume extensions that also causes noise, odour, ground and atmospheric pollution. These taxes are continuously increasing based on the type of waste. For instance, tax for combustible waste has been increased from 15 to €50/ton between 1993 and 1997, up to €75/ton in 2007 while all environmental taxes have been increased by 50% from July 2015 (Bartelings et al., 2005). Additionally, landfilling may also cause land sliding risks which can be dangerous for human life and property. For example, on 20<sup>th</sup> December 2015, 73 people were killed and 33 buildings were destroyed due to a landslide in a China's city. It was found that the landslide in Shenzhen was caused by a huge pile of demolished construction waste (Yang et al., 2017).

### **2.4 Manganese alloy production and associated problems**

There are 118 chemical elements exists in the periodical table developed by the Russian chemist Dmitri Mendeleev in 1869 who categorized them into metals, non-metals, semi-conductor and inert gasses. Manganese (Mn) is located in the periodic table at 25<sup>th</sup> atomic number, it was discovered by Johann Gahn in 1774, and considered as 12<sup>th</sup> most abundant element on earth crust beside 4<sup>th</sup> most abundant metal (Tangstad,



2013). According to International Manganese Institute (IMnI), it is estimated that the current world Mn reserves including low grade ores accounts several billion tons while those with high grade ores (Mn content > 44%) reached 680 million tons of ore in 2011 from which manganese alloy production was noted to be 17.7 MMT. As per 2009 statistics of world Mn reserves and production (in MMT) were respectively as follows in the following Mn resources rich countries: Ukraine (140 and 0.31), South Africa (130 and 1.3), Australia (87 and 1.6), India (56 and 0.96), Gabon (52 and 0.81), China (40 and 2.4), Brazil (29 and 2.4), Brazil (29 and 0.99) while remaining countries accounts for negligible reserves and 1.2 MMT production, as illustrated in **Figure 2.4**. Among the global manganese alloy production, about 90-93% is mainly utilized in steel making as there is no satisfactory substitute of manganese while rest of the manganese is consumed in manufacturing portable batteries, aluminium-based beverage cans, agricultural pesticides, electrical circuits, animal fertilizers, colorants and pigments, oxidizing agent, firework and matches leather tanning and medicines (IMnI, 2018).

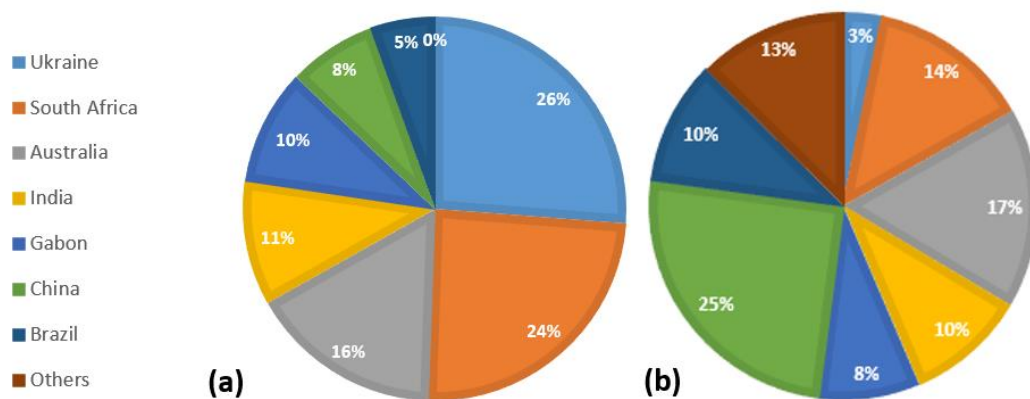


Figure 2.4 2009 statistics of world (a) Mn reserves and (b) production [Adapted: IMnI (2018)]

### 2.4.1 Ferroalloy production process

Blast furnace and submerged electric arc furnace (EAF) are basically two methods for the production of manganese alloy from either high, medium or low-grade ore (Singh et al., 2020). Ferroalloy production activities include raw material handling

(procurement, stockpiling, feeding to storage bin), transportation to EAF, mixing, storage in furnace bins, smelting, tapping, casting and cooling and product handling (slag and metal transportation and finishing), as detailed by the flowchart in [Fig 2.5](#).

A graphical overview of the flow of raw material in a typical silico-manganese ferroalloy plant is also depicted in [Figure 2.6](#). To control the Mn dust emissions during the entire manufacturing process, baghouse filters are placed at each of the smelting, tapping, ladle, casting, crushing and screening areas (Hernández-Pellón et al., 2017). However, during the conversion of manganese ore into manganese alloy, about 15% of manganese is lost in the form of slag or fume while the remainder is chiefly utilized in manufacturing crude steel and limited quantity in other things. It is reported that an Indian plant generates 50,000 t of slag from 60,000 t of annual alloy production such that around 800 to 900 kg of slag per ton of ferroalloy manganese production and required to daily dispose 200 t of slag (Rai et al., 2002).

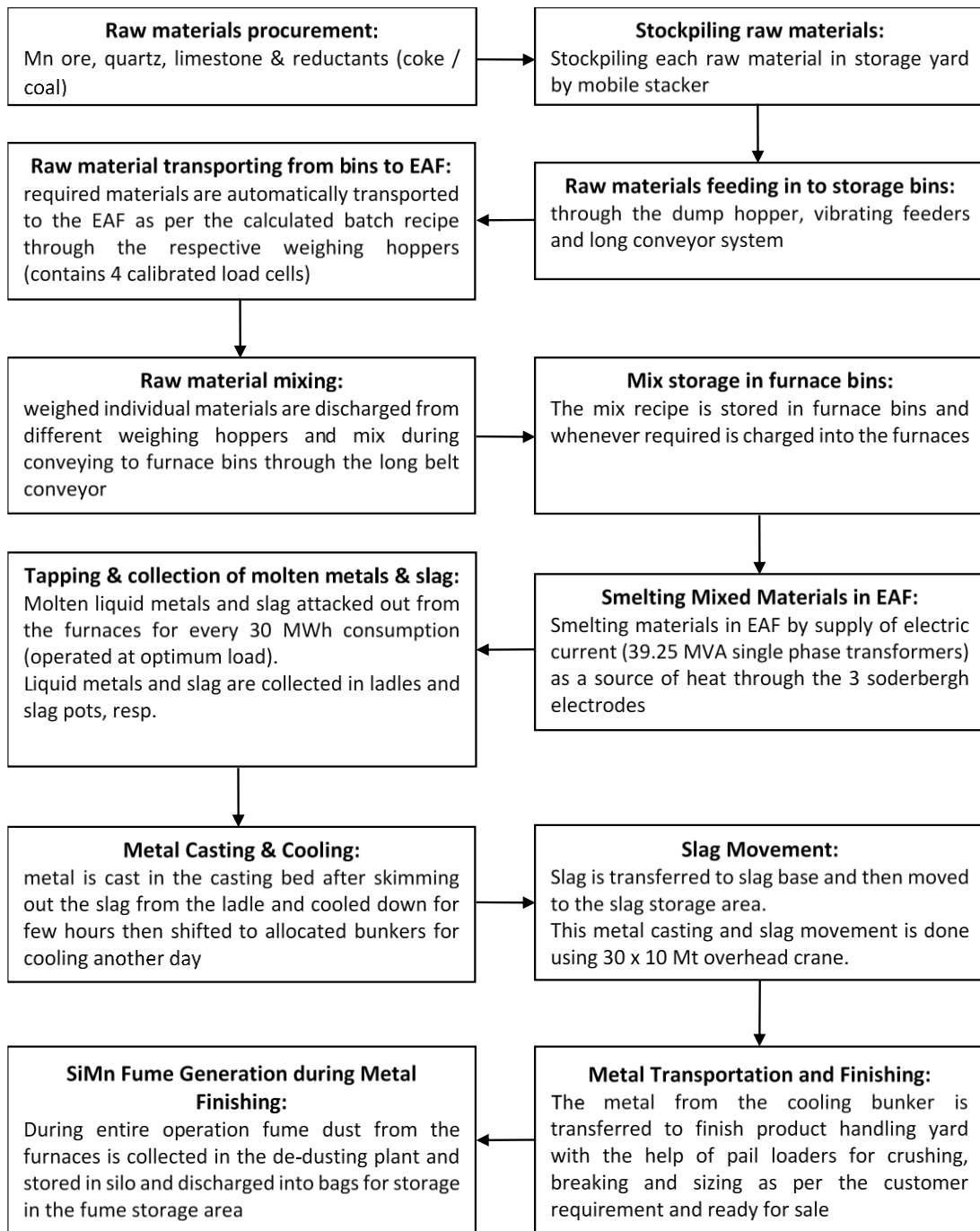


Figure 2.5 Flow chart detailing the production process of FeMn and SiMn at a typical ferroalloy plant  
[Courtesy: [sabayek.com/virtual tour](http://sabayek.com/virtual%20tour)]

It is further estimated that approximately 1.2 to 1.4 tonne of slag is generated for every tonne of SiMn alloy production such that about 10 million tonnes of SiMn

slag is annually produced (Thomas and Gundewar, 2014). As per 2012 statistics of IMnI, 14.8 MMT SiMn slag was generated per year in the world.

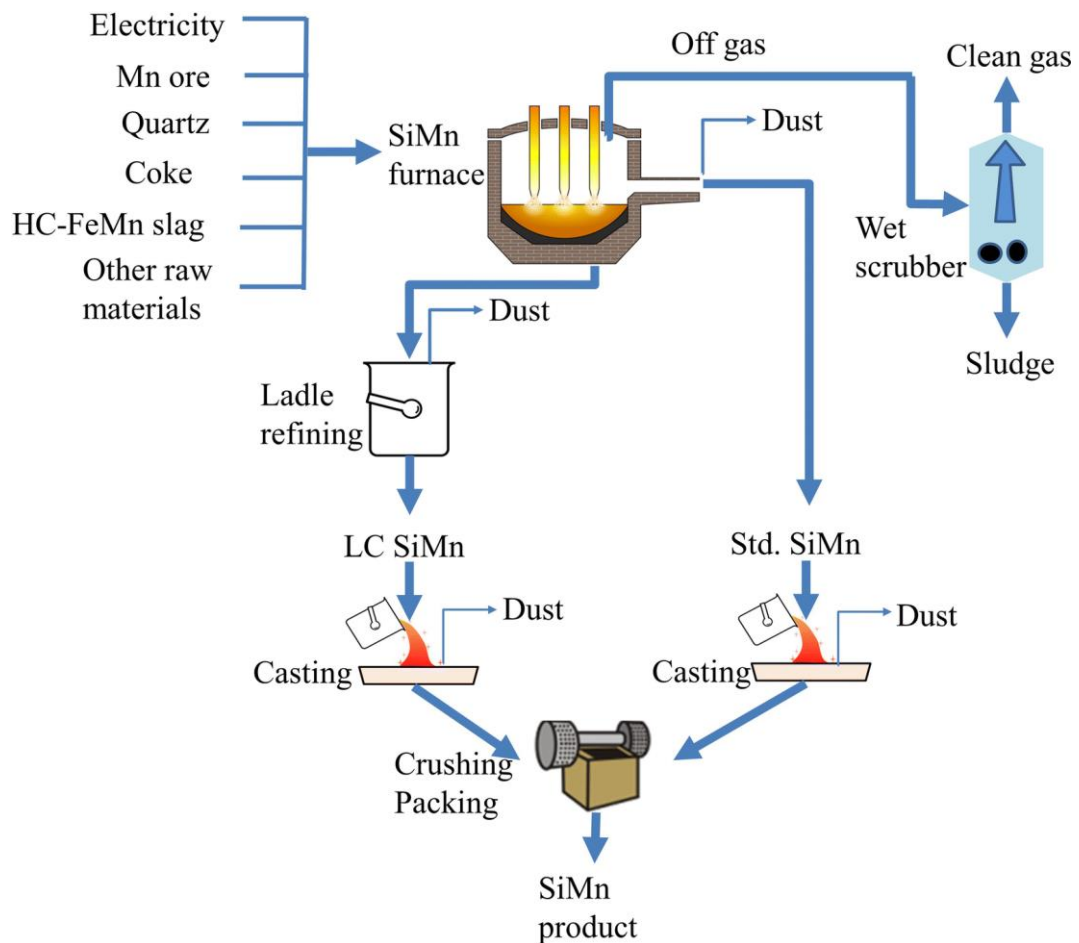


Figure 2.6 Schematic illustration of flow of raw materials in a typical ferroalloy plant  
[Courtesy: Ma et al. (2018)]

High carbon ferromanganese (HC FeMn), refined grades with medium carbon (Ref or MC FeMn) or low carbon (LC FeMn) and silico-manganese (SiMn) are the three grades of ferromanganese alloy that are used in manufacturing steel that constitute 65-79%, 80-81% and 60-77% of Mn content, respectively. Among these grades, 56% of total manganese alloy production accounts for SiMn production which requires low grade ore and used for making 50% of world construction reinforcing steel. Total world manganese alloy production in 2000 and 2008 for HC FeMn, Ref FeMn and SiMn estimated (in MMT) as 3.35 and 4.73, 0.74 and 1.12, 3.77 and 7.85,

respectively, as shown in [Figure 2.7](#) (IMnI, 2018). The worldwide increase in manganese alloy over the years is due to the constantly increased demand of steel.

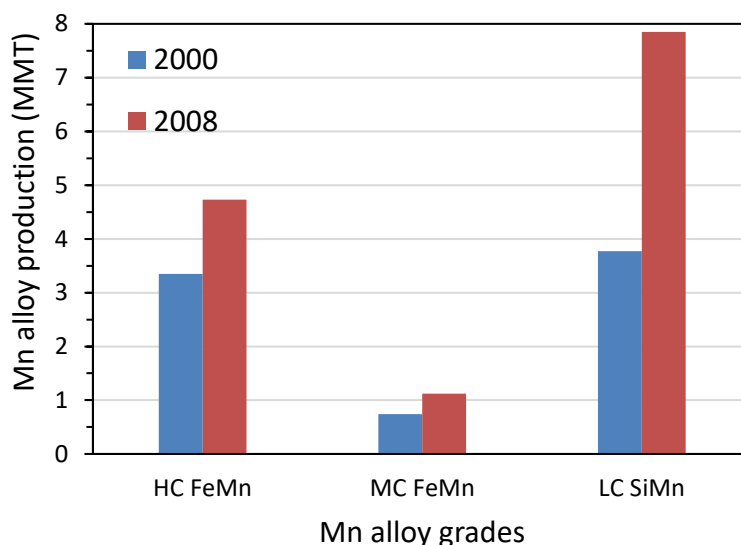


Figure 2.7 World Mn alloy production of different grades  
[Adapted: IMnI (2018)]

#### 2.4.2 Mn concentration in the vicinity of some ferroalloy plants

Ferroalloy industries discharge Mn to the atmosphere in the form of aerosols or suspended particulate matter that are generated from several ferroalloy production activities besides their by-products such as SiMn slag and SiMn fume are separately collected and stored in the designated plant areas. Therefore, to control anthropogenic activities in these plants that leads to high concentration of Mn in industry-surrounding air, World Health Organization (WHO) has set an annual limiting value of 150 ng Mn/m<sup>3</sup>. However, this limit is widely violated by several ferromanganese refineries, as tabulated in [Table 2.1](#).

Table 2.1 Statistics of Mn concentration in the vicinity of some ferroalloy plants

Author(s)	Ferroalloy plant location	Average annual Mn concentration in air (ng/m <sup>3</sup> )	Effectuated plant vicinity (km)	Inhabitants	Year
Haynes et al. (2010)	Marietta town, USA	203	7.3 (north, north-east)	14,515	-
Ledoux et al. (2006)	Agglomeration Community of Boulogne, France	7560	-	120,000	-
Querol et al. (2007)	Cantabria, northern Spain	4 – 23	-	-	-
Moreno et al. (2011)	Santander, northern Spain	166	7 (north-east)	174,000	2007
CIMA (2006)	Maliaño, Spain	781	-	10,000	2005
CIMA (2010)		1072			2009
Arruti et al. (2010)	Santander, northern Spain ( <i>Mn reduction after corrective measures</i> )	49.1	-	-	2008
Ruiz et al. (2014)		31.5	-	-	2009
Pellón and Olmo (2016)	Maliaño, Spain	714	-	-	2015

### 2.4.3 Health problems associated with Mn exposure

Medical researchers found that only limited Mn containing nutrient is vital for human body in the skeleton growth, metabolic function, regulating the immune and nervous system (Santamaria, 2008) as well as it helps in stabilizing reproduction of hormone system and restricts cellular oxidative type of stresses (Freeland-Graves et al., 2014; Keen et al., 2000). On the contrary, overexposure to airborne Mn can lead to several negative health consequences when inhaled and it primarily influences the neurological system including motor (muscular) and cognitive loss (Lodge Jr, 1988; WHO, 2000). Development of manganism or manganese poisoning resulting from chronic exposure to Mn is also reported which somehow resembles to Parkinson's

disease (Flynn and Susi, 2009; Kwakye et al., 2015; Park, 2013). Furthermore, elevated Mn exposure to children and old age people are particularly prone to lower IQ level, reduced body weight, hyperactivity disorder and sensory deficit (Todd et al., 2003).

## **2.5 Remedy of recycling solid wastes in construction industry**

It is highly recommended to make safe disposal strategy for the agro-industrial waste in order to remediate it by eco-friendly and cost-effective manner. One of the effective solutions is to recycle those solid waste at construction industry for the dual advantage of sustainable construction practices and reducing the landfill / open-field burnings. This can be done by replacing traditional cement with waste materials partly or 100% by means of alkali-activation technology, incorporating as fine or coarse aggregate replacement, or strengthening concrete as a fibre addition. In this regard, concrete technologists have started utilizing following agricultural tree waste materials (Aprianti et al., 2015) in concrete making such as from oil palm, date palm, rice husk, sugarcane bagasse, wheat straw, coconut coir, corncob, elephant grass, bamboo, olive waste, etc. Moreover, industrial by-products (Buchwald and Schulz, 2005; Nasir et al., 2016) from iron/steel – ground granulated blast furnace slag, ferrosilicon – silica fume, coal electric power generation plants – fly ash and superpozz, as well as natural supplementary cementitious materials like natural pozzolan and metakaolin have also been extensively used. However, the need of identifying other potential waste products and improvement in existing materials and technology is always present. For instance, silico-manganese (SiMn) fume is one of the sparingly focused material in the literature that consists of excess amount of manganese oxide (MnO) and silica (SiO<sub>2</sub>). This waste